Application of the ISAF-RT Integrated Stress Analysis Framework to the Gorges du Verdon (Southwestern French Alps): In-Situ Stress State, Tunnel Geomechanics, and Comparative Evaluation with Barton's Q-System

Alessandro Calvi[1]

[1] Enel Green Power SpA, Torino, Italy — E-mail: alessandro.calvi84@gmail.com

Abstract

The Gorges du Verdon (Haute-Provence, SW French Alps) constitute a spectacular deep fluvial canyon incised into Upper Jurassic to Lower Cretaceous Tithonian limestones of the Castellane fold-and-thrust belt, a region characterised by active thin-skinned compression (~0.1 mm/yr uplift), a complex network of N–S and E–W fault systems, and topographic relief of 300–700 m. Recent cosmogenic ^{36}Cl exposure dating by Cardinal et al. (2024) has quantified river incision rates of 0.06–0.20 mm/yr for the Late Pleistocene (60–15 ka), with a marked acceleration to 0.90 ± 0.53 mm/yr at the glacial-interglacial transition (16–15 ka). This paper presents the first application of the Integrated Stress Analysis Framework for Rock Tunnels (ISAF-RT; Calvi, 2026) to the Verdon massif, through a hypothetical road tunnel (T-VD1: D = 10.5 m, length 4.6 km, maximum overburden H = 470 m) crossing the gorge axis at the Samson Corridor.

Keywords: ISAF-RT; in-situ stress; Gorges du Verdon; Castellane arc; Tithonian limestone; Q-system; Barton; tunnel geomechanics; thrust-faulting regime; Convergence-Confinement Method; Kirsch solution; K_0 ratio; cosmogenic dating; rock mass classification

1. Introduction

Deep fluvial gorges carved into the limestones of the subalpine chains represent some of the most geotechnically demanding landscapes in the Western Mediterranean. The Gorges du Verdon (Haute-Provence, southeastern France), with canyon walls rising 250–700 m above the Verdon River and a gorge length exceeding 20 km, offer a paradigmatic example of this landscape type. Their development is governed by the interplay of regional tectonic uplift, climate-driven river incision, and the mechanical anisotropy of the Mesozoic carbonate sequence forming the canyon walls—a sequence systematically characterised by Cardinal et al. (2024) through cosmic-ray exposure (CRE) ^{36}Cl dating and geomorphological analysis.

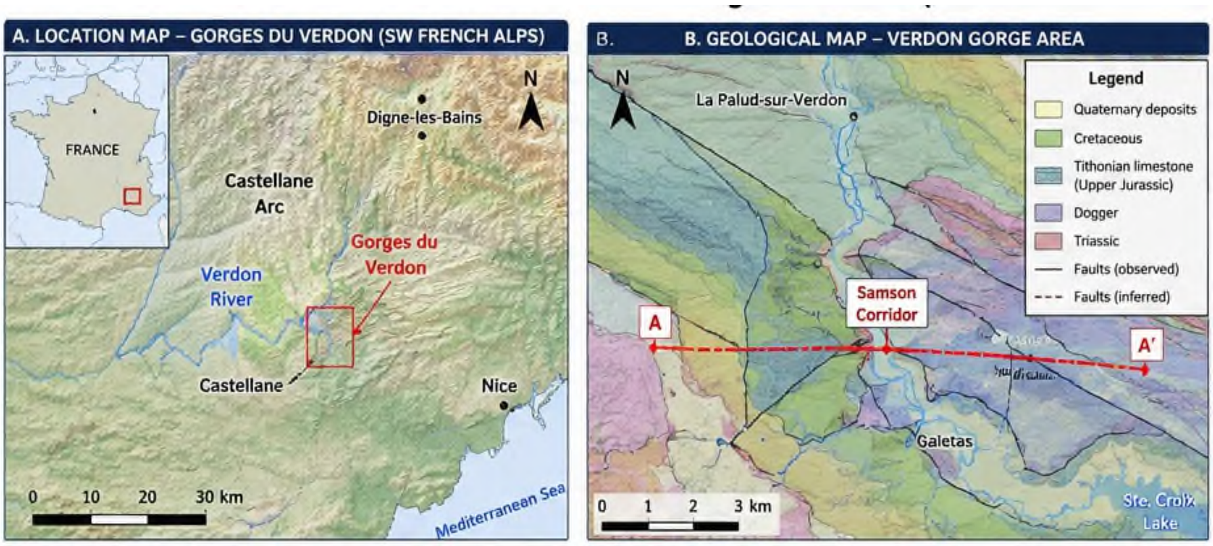

Figure 1. Regional and geological setting of the Gorges du Verdon and the conceptual T-VD1 tunnel corridor.

The design of underground infrastructure in mountainous and tectonically active terrain requires rigorous understanding of the pre-excavation in-situ stress state. In fold-and-thrust belt settings, such as the subalpine chains of the Western Mediterranean, horizontal stresses generated by ongoing compression can substantially exceed the vertical overburden stress, creating conditions that standard empirical classification systems—developed predominantly from Scandinavian hard-rock experience—are not calibrated to handle (Zoback, 2010; Kaiser et al., 1996). This mismatch is a recognised source of systematic errors in tunnel support design in the Alps, Apennines, and Pyrenees.

Cardinal et al. (2024) provide the first high-resolution geomorphological chronology for the High Verdon Gorges (HVG), based on ^{36}Cl surface exposure dating at three sites (Samson Corridor, La Mescla, Galetas). Their dataset constrains river incision rates to 0.06–0.20 mm/yr for the Late Pleistocene (60–15 ka), with a transient acceleration to 0.90 ± 0.53 mm/yr associated with deglaciation flood discharge changes (16–15 ka). These incision rates define the vertical strain budget of the massif and provide essential constraints for interpreting the contemporary stress field.

This paper fills the geomechanical knowledge gap by applying the Integrated Stress Analysis Framework for Rock Tunnels (ISAF-RT) recently published by Calvi (2026)—which bridges reservoir geomechanics stress characterisation techniques (Extended Leak-Off Tests, acoustic televiewer logging, Zoback stress polygon) with tunnel engineering tools (Kirsch, Kastner, Hoek-Brown, Convergence-Confinement Method) within a probabilistic Observational Method framework—to a hypothetical tunnel scenario (T-VD1) crossing the gorge axis at the Samson Corridor section. ISAF-RT has been validated against the Brenner Base Tunnel (55.5 km, overburden ~1850 m) and A1 Apennine Highway tunnels (4.5 km, overburden 100–400 m), yielding support savings of approximately €45 million at the BBT through adaptive feedback (Calvi, 2026).

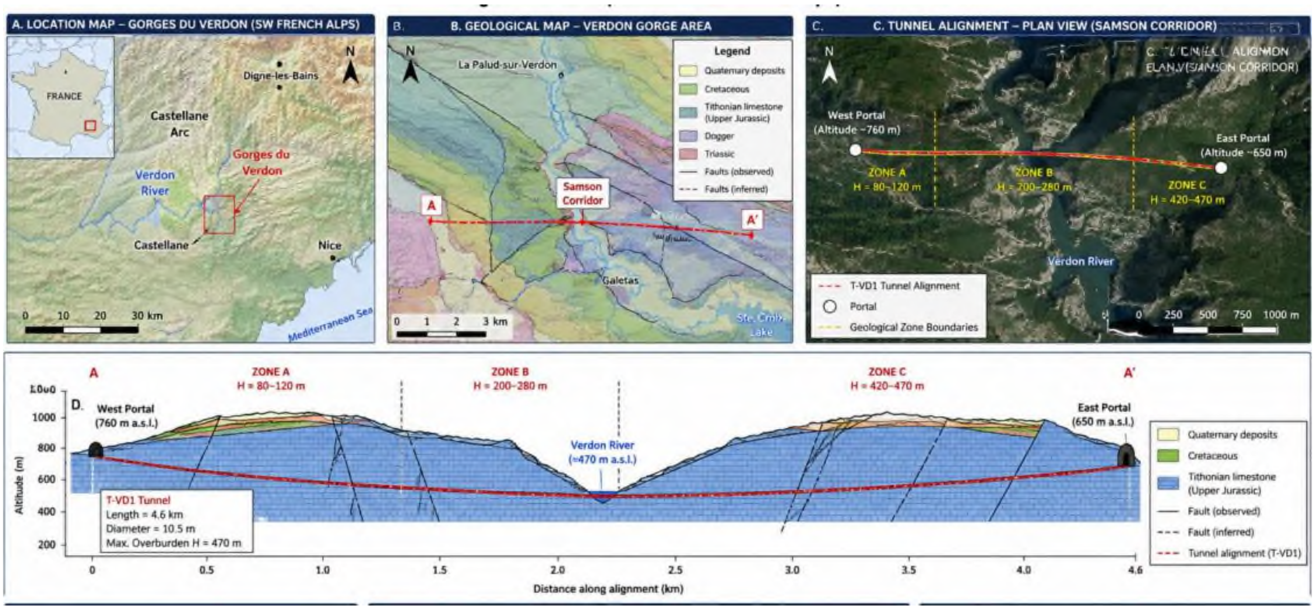

Figure 2. Conceptual T-VD1 tunnel alignment, longitudinal profile and geomechanical zoning.

Figure 3. Conceptual tunnel cross-section, topographic setting and Zone C in-situ stress regime.

The ISAF-RT results are compared systematically with Barton's Q-system (Barton et al., 1974; Barton, 2002), the most widely used empirical classification tool in tunnel design, applied to the same three geological zones along T-VD1. The aims are: (i) to quantify the discrepancy in support demand between the two approaches in a compressional stress regime; (ii) to identify the physical mechanisms responsible for the discrepancy; and (iii) to propose a practical integration strategy exploiting the strengths of both methods.

2. Geological Setting of the Gorges du Verdon

2.1 Stratigraphy and Lithological Units

The High Verdon Gorges expose a near-complete Mesozoic sedimentary sequence of the Alpine foreland. The gorge-forming unit is the Tithonian limestone (Late Jurassic): massive, reef-derived carbonate with unconfined compressive strength σ_{ci} = 120–160 MPa (central value 140 MPa), Young's modulus E_i = 55–70 GPa, and Geological Strength Index GSI typically 65–80 for intact zone cores. The Kimmeridgian–Oxfordian alternation immediately below has significantly lower geomechanical quality (GSI = 45–60, σ_{ci} = 60–90 MPa) and constitutes the primary source of structurally controlled instability. Upstream, Helminthoid Flysch Nappes overlie the sequence above ~2500 m a.s.l. Downstream, the Valensole conglomerate and Balene Breccia (0.7–1.0 Ma) at the Valensole basin margin provide key chronological anchors for long-term incision rates (Cardinal et al., 2024).

Table 1. Stratigraphic column of the High Verdon Gorges (after Cardinal et al., 2024).

Unit	Age	Lithology	Thickness	GSI / σ_ci	Geomechanical character
Helminthoid Flysch	Late Cretaceous–Eocene	Turbidites, shales	>500 m	50–65 / 80 MPa	Moderately strong
Urgonian Limestone	Barremian–Aptian	Bioclastic platform Lst.	60–120 m	60–75 / 90–140 MPa	Massive, high UCS
Hauterivian Marls	Early Cretaceous	Alternating marls + Lst.	30–80 m	40–55 / 50–70 MPa	Weak; slip surfaces
Berriasian–Valanginian Lst.	Earliest Cretaceous	Thin-bedded limestone	50–100 m	45–60 / 70–90 MPa	Moderate; jointed

Unit	Age	Lithology	Thickness	GSI / σ_ci	Geomechanical character
TITHONIAN LIMESTONE	Late Jurassic (Tithonian)	Massive, cliff-forming	150–250 m	65–80 / 120–160	Very high UCS; gorge walls
				MPa	
Kimmeridgian–Oxfordian	Middle–Late Jurassic	Stratified Lst. + marls	100–200 m	45–60 / 60–90 MPa	Moderate; anisotropic
Bajocian–Callovian	Middle Jurassic	Platform carbonates, dolomite	80–150 m	50–65 / 80–120 MPa	Variable; karstified

2.2 Structural Geology and Tectonic Framework

The Gorges du Verdon are situated at the frontal arc of the Castellane fold-and-thrust belt, a thin-skinned contractional structure developed in two main phases (Cardinal et al., 2024): (1) the Pyrenean phase (Late Cretaceous–Eocene), creating the main thrust ramps with shortening along Triassic evaporite décollement horizons; and (2) the Alpine phase (Oligocene–Late Miocene), propagating the thrust front outward and ultimately emplacing the Digne Nappe during the Late Miocene. The contemporary structural fabric comprises NNE–SSW trending reverse faults (Digne-Castellane arc ramps), N–S extensional faults inherited from Oligocene rifting, E–W to NW–SE blind thrusts (dominant active Pliocene-Quaternary structures; Sébrier et al., 1997), and conjugate strike-slip faults at arc boundaries.

Seismicity in the region is moderate (Mmax ~ 5.5 historically), consistent with a thin-skin thrust regime. The orientation of the maximum horizontal stress SHmax is constrained to approximately N130–150°E (NW–SE), perpendicular to the main Castellane arc ramp direction, from fault plane solutions and borehole measurements in the broader SE France region (Zoback et al., 2003; Sanchez et al., 2010). The conceptual tectonic and geological framework adopted for the T-VD1 analysis is shown in Fig. 4.

2.3 Geomorphological Evolution and Incision Chronology

The incision history of the Verdon River has been reconstructed by Cardinal et al. (2024) through cosmogenic ^{36}Cl exposure dating of polished bedrock strath surfaces at three sites. The results provide critical constraints on the vertical strain budget and tectonic component of the contemporary stress field, and the sampled incision-rate dataset is summarised in Table 2.

Table 2. Cosmogenic Cl incision rate data for the High Verdon Gorges (Cardinal et al., 2024).

Site	n samples	CRE age range	Incision rate	Interpretation
Samson Corridor	11	15–45 ka	0.25 ± 0.17 mm/yr (45–30 ka)	Pre-LGM incision
Samson Corridor			0.18 ± 0.03 mm/yr (30–16 ka)	LGM reduced discharge
Samson Corridor			0.90 ± 0.53 mm/yr (16–15 ka)	Deglaciation flood pulse
La Mescla, Sect. 1	8	60–15 ka	~0.10 mm/yr	Steady long-term incision
La Mescla, Sect. 2	8	60–30 ka	0.06–0.07 mm/yr	Hydraulic widening
Galetas	5	55–15 ka	0.06–0.07 mm/yr	Base-level controlled

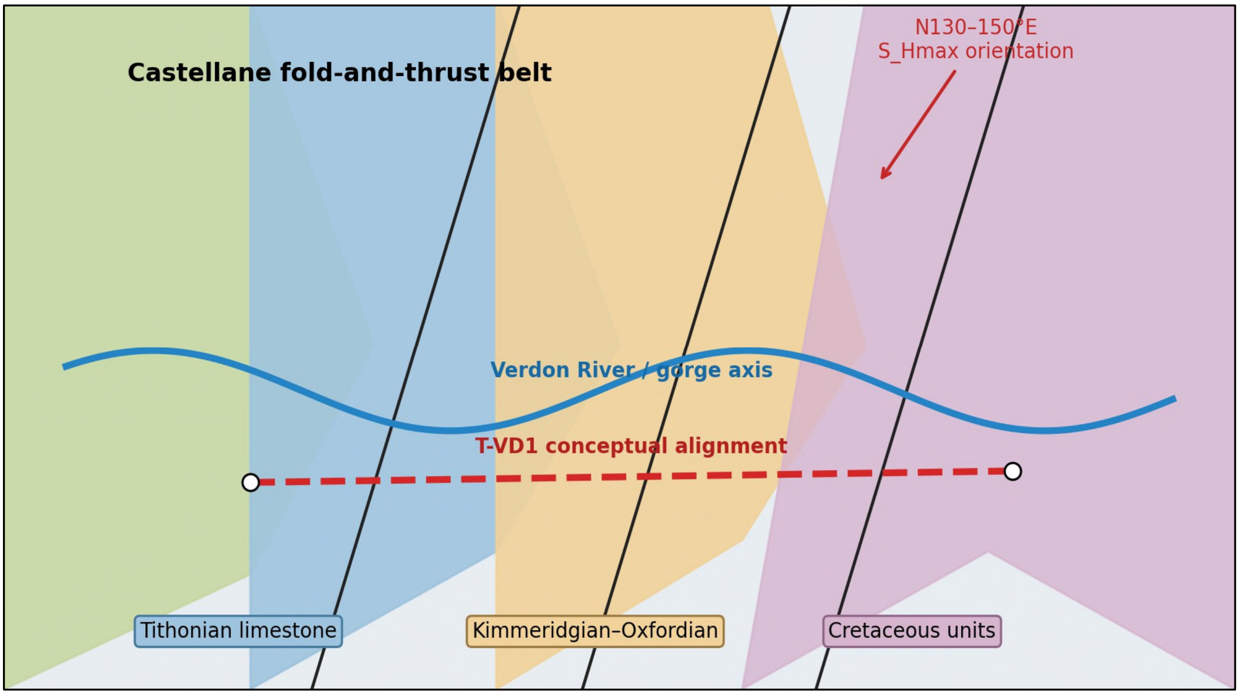

Figure 4. Conceptual tectonic and geological setting used for the T-VD1 analysis

3. ISAF-RT Methodology

3.1 Overview and Conceptual Basis

The Integrated Stress Analysis Framework for Rock Tunnels (ISAF-RT) (Calvi, 2026) is a six-phase sequential methodology bridging reservoir geomechanics stress characterisation with tunnel engineering analytical tools. Its conceptual basis rests on three pillars: (1) physics-based stress constraints via the Zoback (2010) stress polygon, limited by Byerlee's (1978) friction law (μ = 0.6–0.85); (2) systematic in-situ measurement via Extended Leak-Off Tests (ELOTs) and acoustic televiewer (ATV) logging; and (3) probabilistic feedback through Monte Carlo simulations and the Observational Method (Peck, 1969; CIRIA, 1999).

3.2 Phase I: In-Situ Stress Characterisation

Phase I establishes the 3D stress model. The vertical stress is estimated from overburden weight:

$$S_v = \rho \cdot g \cdot H \approx 0.026 \cdot H \text{ [MPa]} \quad (1)$$

where ρ = 2,650 kg/m³ (limestone), g = 9.81 m/s², H = overburden depth [m]. The Sheorey (1994) empirical K_0 model provides the initial estimate of horizontal stress ratio:

$$K_0 = 0.25 + 7 \cdot E_r \cdot (0.001 + 1/H) \quad (2)$$

where Er is the rock mass Young's modulus [GPa]. The frictional equilibrium constraint from Byerlee's law limits the maximum stress ratio:

$$\sigma_1/\sigma_3 \le [(\mu^2 + 1)^{0.5} + \mu]^2 \quad (3)$$

For μ = 0.6: (σ_1/σ_3)_max = 3.12; for μ = 0.85: (σ_1/σ_3)_max = 4.69.

3.3 Phase II: Kirsch Stress Screening

Phase II applies the Kirsch (1898) analytical solution. The maximum tangential stress at the tunnel wall (springline, perpendicular to S_Hmax) is:

$$\sigma\theta{,}max = 3 \cdot S\_Hmax - S_v \quad (4)$$

The Rock Stress Index (RSI) determines the stress severity class:

$$RSI = \sigma\theta{,}max \,/\, \sigma ci = (3 \cdot S\_Hmax - S_v) \,/\, \sigma ci \quad (5)$$

RSI thresholds: <0.15 (negligible), 0.15–0.40 (moderate), 0.40–0.70 (high), >0.70 (severe/squeezing).

3.4 Phases III–IV: Failure Assessment and Plastic Zone

Phase III assesses hydraulic fracturing risk; Phase IV integrates the Hoek-Brown (2002) failure criterion:

$$\sigma_1 = \sigma_3 + \sigma ci \cdot (mb \cdot \sigma_3/\sigma ci + s)^a \quad (6)$$

where mb, s, a are rock mass constants from GSI and disturbance factor D. The Kastner (1962) plastic zone radius:

$$R_p/R = \{[2(P_0(K\phi - 1) + c \cdot \cot\phi)] \,/\, [(1 + K\phi)(P_i(K\phi - 1) + c \cdot \cot\phi)]\}^{1/(K\phi - 1)} \quad (7)$$

The squeezing severity index (Hoek & Marinos, 2000):

$$\varepsilon s\ (\%) = 0.2 \cdot (\sigma cm/P_0)^{-2} \cdot 100 \quad (8)$$

εs classification: <1% no squeezing; 1–2.5% minor; 2.5–5% moderate; 5–10% high; >10% severe.

3.5 Phase V: Convergence-Confinement Method

Phase V applies the Convergence-Confinement Method (CCM) (Panet & Guenot, 1982) to size the support system by coupling the Ground Reaction Curve (GRC), Longitudinal Deformation Profile (LDP), and Support Characteristic Curve (SCC). The equilibrium point (GRC–SCC intersection) must satisfy Pi,equilibrium ≥ Pi,required (Phase IV), and the displacement at equilibrium must lie within the deformation capacity of the chosen lining.

3.6 Phase VI: Long-Term Stability

Phase VI evaluates long-term stability over a 100-year service life, addressing: (a) creep in argillaceous intercalations; (b) seismic loading from the Castellane arc seismic source (M_max ~ 5.5, PGA ~ 0.15g); (c) groundwater changes in karst limestone (seasonal piezometric fluctuations ±0.5–1.0 MPa); and (d) Monte Carlo reliability assessment of the lining against the P90 stress scenario. The Observational Method feedback loop (Phase VI → Phase I) updates the stress model and GSI distribution in real time as monitored convergence data become available during construction (Calvi, 2026).

4. Geomechanical Characterisation of Tunnel Alignment T-VD1

4.1 Tunnel Geometry and Zoning

The hypothetical tunnel T-VD1 is a twin-lane road tunnel (2 × 7.5 m lanes, 4.8 m clearance) with excavated diameter D = 10.5 m (radius R = 5.25 m), oriented approximately N30°W–S30°E (perpendicular to the gorge axis). Total length: 4.6 km. Three geomechanical zones are defined based on depth and lithology: Zone A (portal, 0.0–0.8 km, H = 80–120 m), Zone B (Tithonian with moderate jointing, 0.8–2.1 km, H = 200–280 m), and Zone C (massive Tithonian core, 2.1–3.6 km, H = 420–470 m). The critical zone for tunnel design is Zone C, located beneath the gorge divide at maximum depth. The longitudinal profile and geomechanical zoning of the alignment are illustrated in Fig. 5.

4.2 Rock Mass Parameters

Table 3. Rock mass parameters by tunnel zone (after Hoek et al., 2002; Cardinal et al., 2024).

Parameter	Zone A (H=100 m)	Zone B (H=240 m)	Zone C (H=470 m)	Notes
Lithology	Hauterivian-Berriasian Lst.	Tithonian Lst., jointed	Tithonian Lst., massive	
GSI	45 ± 8	60 ± 5	70 ± 5	Marinos & Hoek (2000)
σ_{ci} (MPa)	80 ± 15	120 ± 20	140 ± 15	UCS intact rock
m_i	9	10	10	Limestone
D (disturbance)	0.5	0.3	0.1	Controlled blasting
m_b	0.98	2.28	3.24	Hoek-Brown (2002)
a	0.508	0.503	0.501	Hoek-Brown (2002)
σ_{cm} (MPa)	3.8	12.9	23.5	Rock mass UCS
E_{rm} (GPa)	8.5	16.2	23.4	Rock mass modulus
φ (equiv., °)	28	38	44	M-C equivalent
c (equiv., MPa)	0.9	3.1	5.6	M-C equivalent

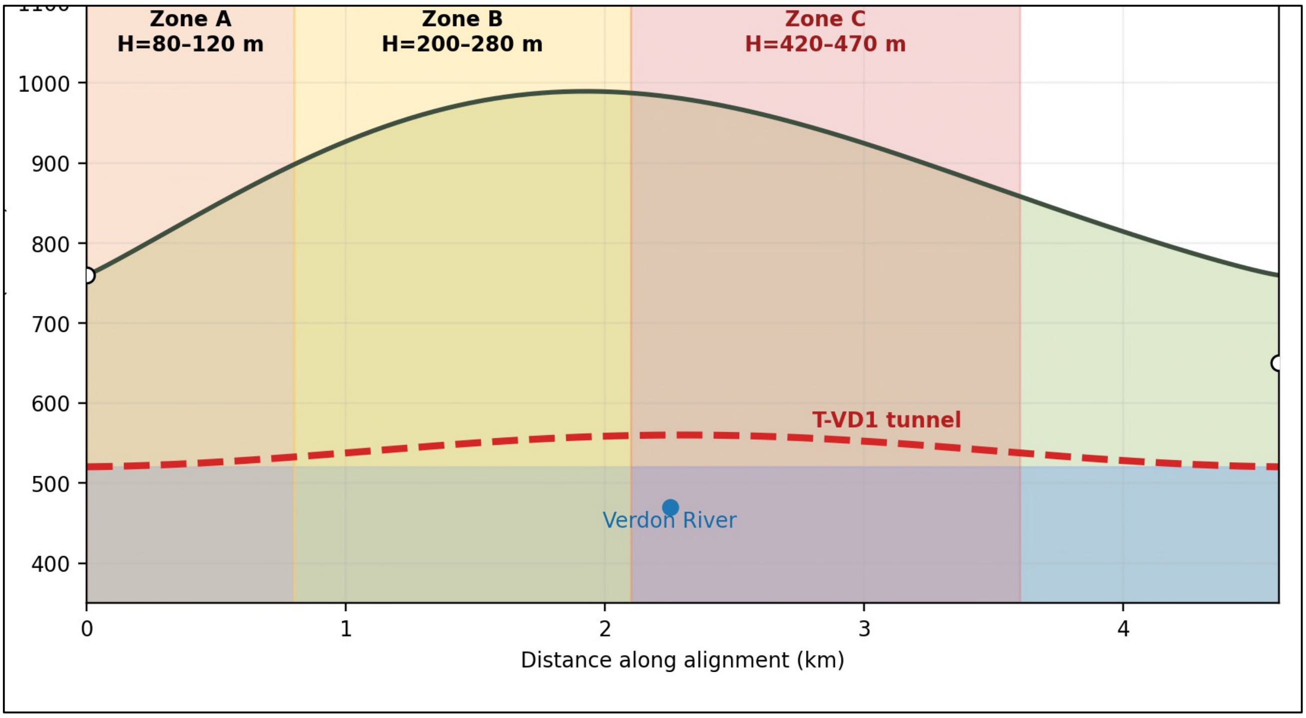

Figure 5. Conceptual longitudinal profile and geomechanical zoning of T-VD1.

4.3 In-Situ Stress Field — Phase I Application

The in-situ stress field is constrained by combining the Sheorey K_0 model (Eq. 2), Byerlee frictional equilibrium bounds (Eq. 3), the regional SHmax orientation (N130–150°E), and the vertical strain rate from the Cardinal et al. (2024) incision chronology. The zoning geometry used in the calculation is illustrated in Fig. 5, while the resulting stress estimates are summarised in Table 4.

Table 4. In-situ stress state by tunnel zone (ISAF-RT Phase I).

Stress parameter	Zone A (H=100 m)	Zone B (H=240 m)	Zone C (H=470 m)
S_v = 0.026·H (MPa)	2.60	6.24	12.22
K_0_min (Byerlee, thrust)	1.40	1.38	1.35
K_0_max (Sheorey upper)	2.10	1.88	1.75
K_0_central (Sheorey)	1.80	1.60	1.54
S_Hmax central (MPa)	4.68	9.98	21.30
S_hmin central (MPa)	3.64	8.61	16.43
S_Hmax range (MPa)	3.64–5.46	8.61–11.73	16.50–21.39
Pore pressure p_u (MPa)	0.50	1.20	4.70
Stress regime	Thrust	Thrust	Thrust

5. Tunnel Stress Analysis: Zone-by-Zone ISAF-RT Application

5.1 Zone A — Portal Section (H = 100 m)

Phase I–II results: S_v = 2.60 MPa; K_0 = 1.80; S_Hmax = 4.68 MPa.

```
σθ,max = 3 × 4.68 − 2.60 = 11.44 MPa
RSI = 11.44 / 80 = 0.143    (low stress influence, borderline)
```

The far-field mean stress P_o = (4.68 + 2.60)/2 = 3.64 MPa barely exceeds σ_cm, generating severe squeezing:

$$\varepsilon s = 0.2 \times (3.8/3.64)^{-2} \times 100 = 18.4\% \quad \text{[SEVERE SQUEEZING]} \quad (9)$$

The Kastner plastic zone radius (P_i = 0): K_φ = (1+sin28°)/(1-sin28°) = 2.77. R_p/R = [(2(3.64×4.55 + 0.9×1.88)) / (3.77×0.9×1.88)]^(1/1.77) = 2.552^0.565 = 1.84. Plastic zone depth from wall: 1.84 × 5.25 − 5.25 = 4.4 m. Required P_i for R_p/R ≤ 1.3: 0.38–0.45 MPa.

5.2 Zone B — Intermediate Section (H = 240 m)

$$\sigma\theta,\text{max} = 3 \times 9.98 - 6.24 = 23.70 \text{ MPa}$$

$$\text{RSI} = 23.70 / 120 = 0.198 \quad \text{(moderate stress)}$$

$$\varepsilon s = 0.2 \times (12.9/8.11)^{-2} \times 100 = 7.9\% \quad \text{[HIGH SQUEEZING]} \quad (10)$$

Kastner: K_φ = 4.21; R_p/R = 1.47; required P_i = 0.35–0.45 MPa.

5.3 Zone C — Deep Central Section (H = 470 m) [Critical Zone]

Full phase-by-phase derivation for the critical design zone. Phase I stress state:

$$S_v = 0.026 \times 470 = 12.22 \text{ MPa} \quad (11)$$

$$K_0 = 0.25 + 7 \times 65 \times (0.001 + 1/470) = 1.673 \quad (12)$$

$$S\_Hmax = 1.75 \times 12.22 = 21.39 \text{ MPa} \quad (K_0\text{,max conservative upper bound}) \quad (13)$$

$$S\_hmin = 1.35 \times 12.22 = 16.50 \text{ MPa} \quad (K_0\text{,min Byerlee frictional lower bound}) \quad (14)$$

Phase II — Kirsch tangential stresses:

$$\sigma\theta,\text{max} = 3 \times 21.30 - 12.22 = 51.68 \text{ MPa} \quad \text{(at tunnel springlines)} \quad (15)$$

$$\sigma\theta,\text{min} = 3 \times 12.22 - 21.30 = 15.36 \text{ MPa} \quad \text{(at crown/invert)} \quad (16)$$

$$\text{RSI} = 51.68 / 140 = 0.369 \quad \text{(moderate-high, approaching high-stress threshold)} \quad (17)$$

Phase IV — Hoek-Brown rock mass constants (GSI=70, σ_ci=140 MPa, m_i=10, D=0.1):

$$mb = 10 \cdot \exp[(70 - 100)/(28 - 14 \times 0.1)] = 10 \cdot e^{-1.128} = 3.24 \quad (18)$$

$$s = \exp[(70 - 100)/(9 - 3 \times 0.1)] = e^{-3.448} = 0.0317 \quad (19)$$

$$\sigma cm = 140 \times (0.0317)^{0.501} = 23.5 \text{ MPa} \quad (20)$$

Squeezing severity (P_o = (21.30+12.22)/2 = 16.76 MPa):

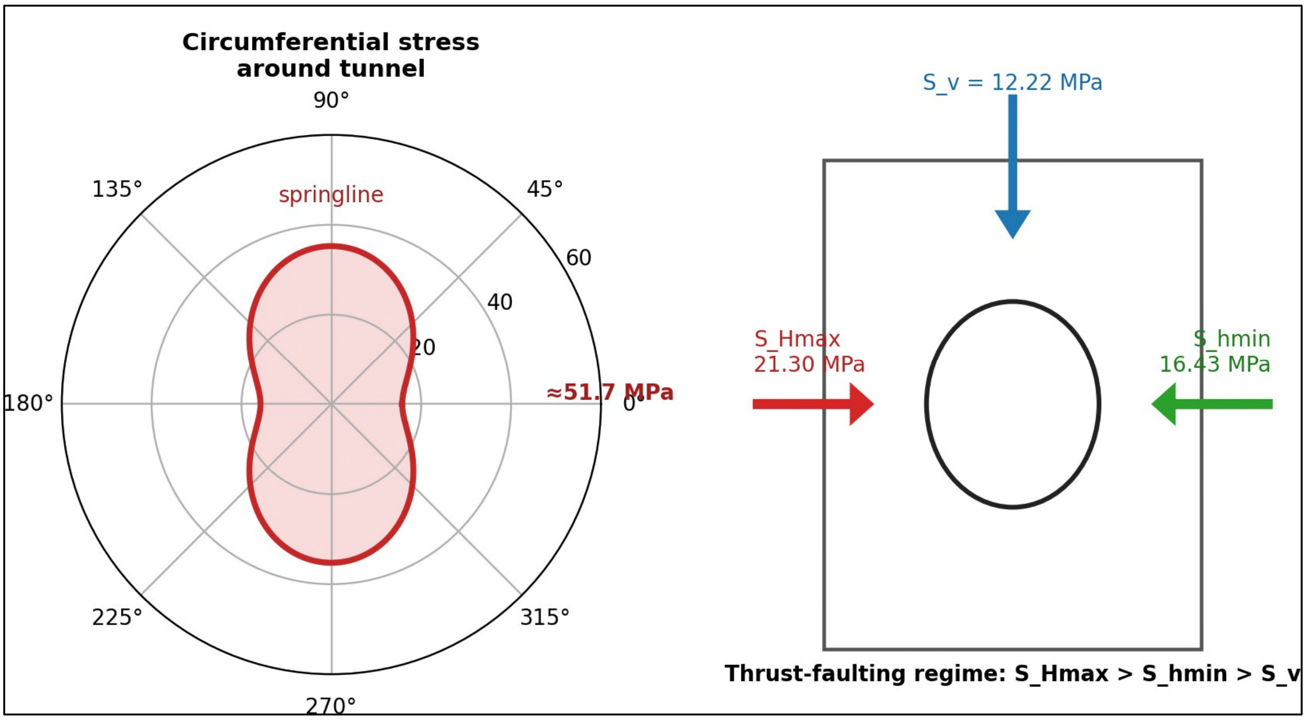

Figure 6. Zone C in-situ stress tensor and Kirsch stress concentration.

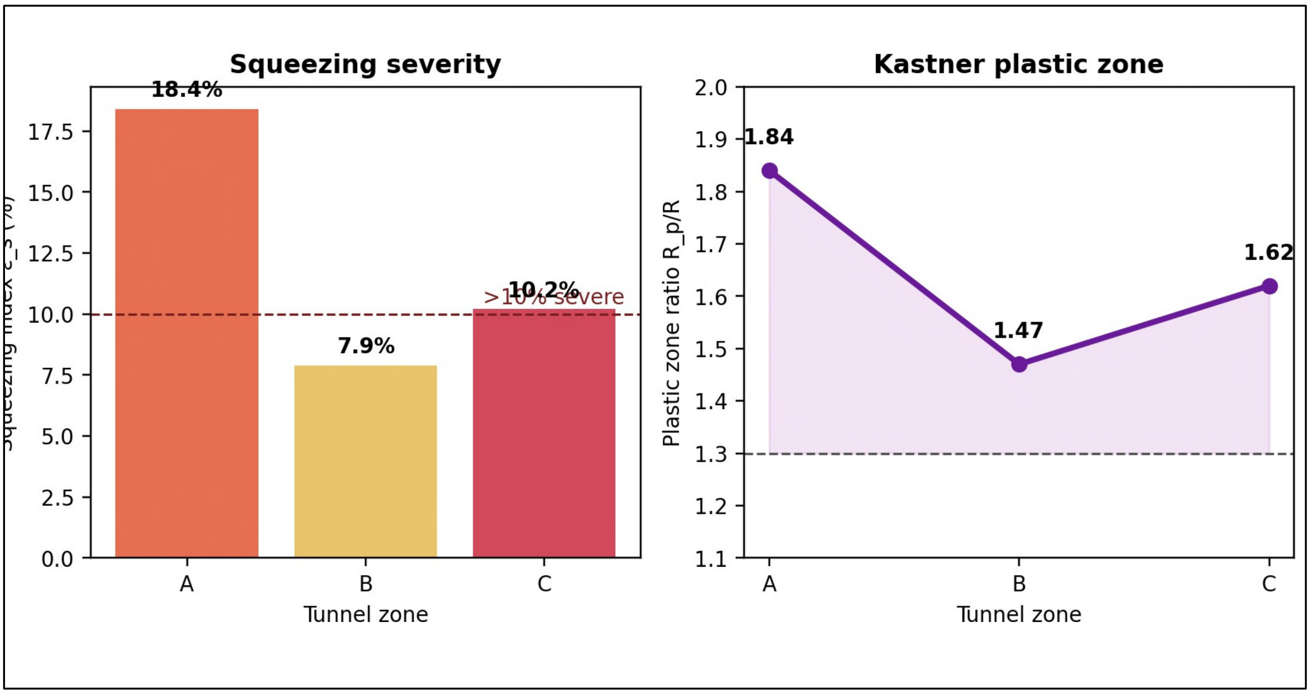

Figure 7. Predicted squeezing and plastic-zone development along T-VD1

$$\varepsilon s = 0.2 \times (23.5/16.76)^{-2} \times 100 = 10.2\% \quad [\text{HIGH–SEVERE SQUEEZING}] \quad (21)$$

Kastner plastic zone (Mohr-Coulomb equiv.: φ=44°, c=5.6 MPa; K_φ=(1+sin44°)/(1-sin44°)=5.55):

$$R_p/R = [(2(16.76 \times 4.55 + 5.6 \times 1.036)) / (6.55 \times 5.6 \times 1.036)]1/4.55 = [4.32]^{0.220} = 1.62 \quad (22)$$

$$R_p = 1.62 \times 5.25 = 8.51 \text{ m} \rightarrow \text{plastic zone extends 3.26 m from tunnel wall} \quad (23)$$

$$P_i\text{,required} = 0.62\text{–}0.83 \text{ MPa} \quad [\text{for } R_p/R \leq 1.3\text{; P10–P90 stress range}] \quad (24)$$

6. Support Design via the Convergence-Confinement Method (Phase V)

The CCM equilibrium for Zone C is established following the Carranza-Torres & Fairhurst (1999) analytical solution for the Hoek-Brown GRC. Table 5 summarises the CCM results for the P50 stress scenario (K_0 = 1.54, S_Hmax = 18.82 MPa).

Table 5. CCM results for Zone C (H = 470 m, P50 stress scenario).

Quantity	Value	Notes
Max elastic radial displacement u_el	31.2 mm	At wall, before yielding
Total radial displacement (no support)	156.4 mm	Full squeezing
Critical internal pressure P_cr	3.84 MPa	Onset of plastic zone
Required P_i (central, R_p/R ≤ 1.3)	0.72 MPa	P10: 0.62 MPa, P90: 0.83 MPa
Lining installation distance from face	10.5–16 m (1.0–1.5 × D)	Heavy squeezing protocol
Pre-release displacement at installation	~52–65 mm (33% pre-release)	LDP (Vlachopoulos & Diederichs, 2009)
Residual displacement for lining	~104 mm	To be absorbed by lining system
Recommended lining	200 mm SFRS + 6-cm yielding slots + 450	Heavy ductile support

The Zone C stress state and stress concentration are visualised in Fig. 6.

uantity	Value	Notes
	mm RC lining	
Lining capacity P_i,max	1.05 MPa	After upgauging from 0.85 MPa
Safety factor (P_i,max / P_i,P90)	1.05 / 0.83 = 1.27	Adequate after yield slots

The recommended support system for Zone C comprises: (1) immediate support of 200 mm steel-fibre-reinforced shotcrete (SFRS, f_ck = 30 MPa) applied in two 100 mm passes with 6-cm yielding slots at 2-m intervals (ductile ring concept; Kovári, 1998); (2) pattern Swellex/IBO friction bolts (L = 6 m, 1.2 × 1.2 m grid, fully grouted); and (3) a 450 mm reinforced concrete secondary lining cast after convergence rate falls below 2 mm/month. Systematic perforated HDPE drainage pipes are specified to limit piezometric buildup in the karst limestone. For Zone B, a lighter lining (100 mm SFRS + 350 mm RC) is specified (P_i,capacity = 0.45 MPa). For Zone A, a full-face umbrella arch pre-support is required given severe squeezing in the fractured portal limestone despite shallow overburden.

7. Application of Barton's Q-System

7.1 Q-System Parameterisation

The Q-system (Barton et al., 1974; Barton, 2002) is applied to the same three zones. The anisotropic stress field SRF formula (Barton, 2002) is used throughout:

$$Q = (RQD/J_n) \times (J_r/J_a) \times (J_w/SRF) \quad (25)$$

$$SRF = 31 \cdot (\sigma_1/\sigma_3)^{0.3} \cdot (\sigma_c/\sigma_1)^{(-1.2)} \quad (26)$$

where σ_1 = S_Hmax, σ_3 = S_v, σ_c = σ_ci. Table 6 gives the full parameterisation.

Table 6. Q-system parameter assignment by zone.

Parameter	Zone A (H=100 m)	Zone B (H=240 m)	Zone C (H=470 m)	Rationale
RQD (%)	40	70	85	GSI–RQD correlation
J_n	12	9	6	Zone A: 3 sets+random; B: 3 sets; C: 2 sets
J_r	1.5	2.0	2.0	Smooth–undulating,

Parameter	Zone A (H=100 m)	Zone B (H=240 m)	Zone C (H=470 m)	Rationale
				planar–undulating
J_a	2.0	1.0	1.0	Zone A: slightly altered; B,C: tight calcite
J_w	0.66	0.66	0.50	A,B: minor inflows; C: karst possible
σ_1/σ_3 ratio	1.80	1.60	1.74	From Phase I stress state
$(\sigma_1/\sigma_3)^{0.3}$	1.182	1.147	1.175	Eq. (26) factor 1
$(\sigma_c/\sigma_1)^{(-1.2)}$	0.0328	0.0490	0.0984	Eq. (26) factor 2
SRF	1.20	1.74	3.58	Eq. (26) result
Q	1.375	5.90	3.97	Eq. (25) result
$Q_c = Q \times \sigma_{ci}/100$	1.10	7.08	5.56	Normalised Q
$E_m = 10 \cdot Q_c^{(1/3)}$ (GPa)	10.3	19.2	17.7	Barton (2002)
E_{rm} (ISAF-RT, GPa)	8.5	16.2	23.4	Hoek-Brown; comparison

7.2 Q-System Support Recommendations

Using the Grimstad-Barton (1993) Q-support chart with ESR = 1.0 (permanent road tunnel) and equivalent span = D/ESR = 10.5 m:

Table 7. Q-system support recommendations by zone (Grimstad-Barton, 1993 chart).

Zone	Q	Q_c	Span/ESR	Support category	Shotcrete	Bolt spacing	Equiv. P_i (MPa)
A	1.38	1.10	10.5 m	Cat. 7: SFRS + systematic bolts	120 mm fibre-RC	1.3 × 1.3 m, L=4 m	0.39–0.50
B	5.90	7.08	10.5 m	Cat. 5: SFRS + spot bolts	80 mm SFRS	1.7 × 1.7 m, L=3 m	0.18–0.24

Zone	Q	Q_c	Span/ESR	Support category	Shotcrete	Bolt spacing	Equiv. P_i (MPa)
C	3.97	5.56	10.5 m	Cat. 6: SFRS + systematic bolts	90 mm SFRS	1.5 × 1.5 m, L=3.5 m	0.28–0.38

The deformation modulus from Q-system (Eq. 36: $E_m = 10 \cdot Q_c^{(1/3)}$): Zone C gives E_m = 17.7 GPa vs. ISAF-RT Hoek-Brown E_{rm} = 23.4 GPa (factor ~1.3 difference). The seismic velocity for Zone C: $V_p \approx \log(Q_c) + 3.5 = \log(5.56) + 3.5 = 4.25$ km/s, consistent with moderate-quality massive limestone.

8. Comparative Analysis: ISAF-RT vs. Barton's Q-System

8.1 Quantitative Comparison of Support Demand

Table 8 synthesises the support demand computed by ISAF-RT (Phases II–V) and estimated from the Grimstad-Barton Q-support chart (Grimstad and Barton, 1993) for all three zones. The two methods display converging results at the portal (Zone A) but diverge systematically with depth, reaching a factor of 2.1–2.2 in the deep Zone C.

Table 8. ISAF-RT vs. Q-System: Quantitative Support Demand Comparison

Quantity	Zone A (H=100 m)	Zone B (H=280 m)	Zone C (H=470 m)	Trend
ISAF-RT P_i,required (MPa)	0.38–0.45	0.35–0.45	0.62–0.83	Increases with depth/K_0
Q-system P_i,equivalent (MPa)	0.39–0.50	0.18–0.24	0.28–0.38	Peaks at portal, then falls
ISAF-RT / Q-system ratio	~0.9	~1.8	2.1–2.2	Diverges strongly at depth
RSI (ISAF-RT)	0.14	0.20	0.37	Moderate throughout
ε_s squeezing index (%)	18.4 (Severe)	7.9 (High)	10.2–12.9 (High–Severe)	Severe at portal
Q_c (normalised)	1.10	7.08	5.56	Good correlation with GSI
SRF (Barton anisotropic)	1.20	1.74	3.58	Increases with depth
E_rm ISAF-RT vs. Q	8.5 vs. 10.3	16.2 vs. 19.2	23.4 vs. 17.7	Diverges at high GSI

Zone A (portal, H = 100 m, highly fractured Berriasian-Hauterivian limestone): the two methods broadly agree (ratio ≈ 0.9). The Q-system correctly captures the high support demand from the low-Q rock mass. ISAF-RT is marginally lower because, despite the formally severe squeezing index (ε_s = 18.4%), the absolute far-field stress is low (P_o = 3.64 MPa) and the CCM equilibrium is manageable.

Zone B (intermediate, H = 280 m, well-jointed Tithonian limestone): the Q-system significantly under-predicts support demand (ratio ≈ 1.8). This is the first zone where the thrust-regime stress anisotropy (K_0 = 1.60, σ_1/σ_3 = 1.60) drives significant stress concentration at the springlines — a condition captured by the Kirsch RSI and Kastner analysis in ISAF-RT, but only partially penalised by SRF = 1.74. The SRF formula was calibrated primarily against Scandinavian hard-rock tunnels with isotropic to mildly anisotropic conditions (K_0 = 0.8–1.3); its extrapolation to K_0 > 1.5 introduces systematic non-conservatism.

Zone C (deep Tithonian core, H = 470 m): the discrepancy is maximum (ratio 2.1–2.2). ISAF-RT requires P_i = 0.62–0.83 MPa with yielding slot support. The Q-system recommends only 90 mm SFRS with systematic bolting (P_i ≈ 0.28–0.38 MPa, Category 6) — a support level structurally inadequate given the predicted convergence of 104 mm residual displacement. Implementing Q-system support alone in Zone C would lead to lining overstress and potential collapse during construction.

8.2 Physical Interpretation of the Discrepancies

The fundamental source of the ISAF-RT/Q discrepancy in compressional tectonic settings is the different physical representation of stress anisotropy in the two frameworks.

ISAF-RT resolves the full 3D stress tensor (S_v, S_{hmin}, S_{Hmax}) through: (i) Phase I direct measurement of S_{hmin} and indirect inversion of S_{Hmax} from borehole data; (ii) Phase II Kirsch analytical stress transformation providing the actual tangential stress distribution; (iii) Phase IV Kastner plastic zone computation using the exact far-field stress state; and (iv) Phase V CCM equilibrium based on the full plastic zone geometry.

Barton's Q-system encodes stress effects solely through the scalar SRF, which: (i) is derived from empirical correlations with a database dominated by Scandinavian hard-rock tunnels (K_0 = 0.8–1.3); (ii) is applied as a single number regardless of S_{Hmax} orientation relative to the tunnel

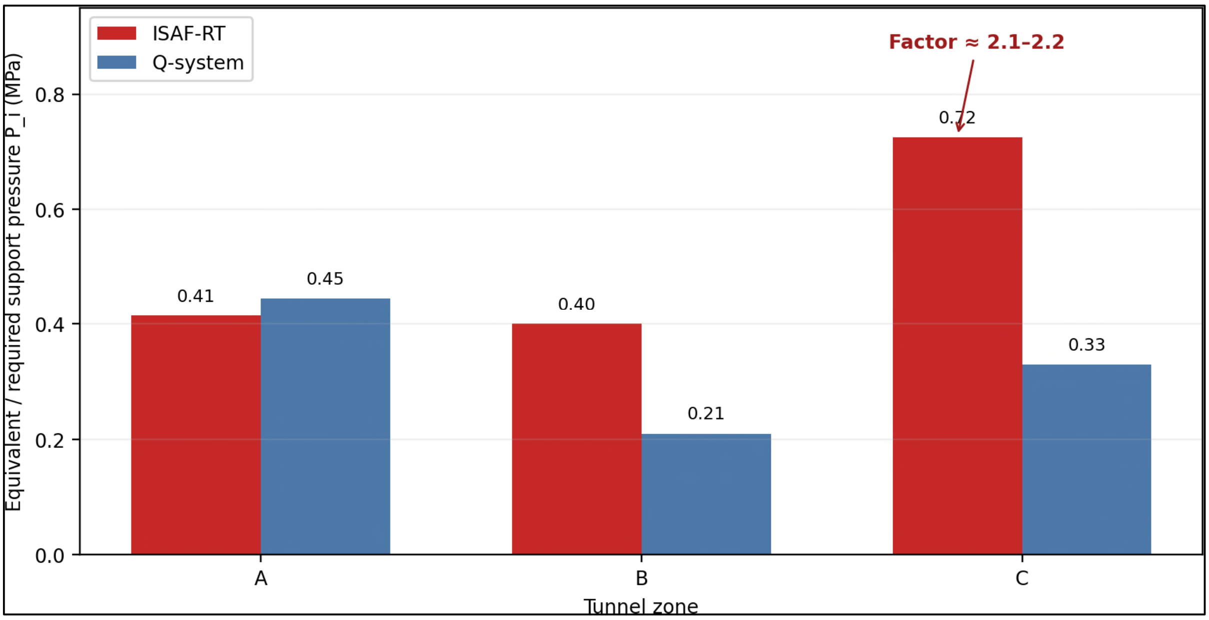

Figure 8. Comparison of support demand between ISAF-RT and Barton's Q-system.

axis (two tunnels with identical Q but 90° vs. 45° crossing of S_Hmax generate entirely different stress concentrations, indistinguishable to the SRF); and (iii) lacks physical connection to the Kirsch stress concentration factor, the Kastner plastic zone radius, or the Hoek-Brown failure envelope.

As demonstrated in the Zone C analysis, SRF = 3.58 reduces Q but does not fully capture the 2.5× stress amplification at the tunnel springlines (σ_θ,max = 51.68 MPa vs. σ_cm = 23.5 MPa). The Q-system's implicit assumption that support demand scales as Q^{-1} breaks down when plastic zone development is driven by a stress state where the σ_θ/σ_cm ratio exceeds the Hoek-Brown peak strength threshold in a directionally asymmetric manner.

A secondary discrepancy involves the rock mass deformation modulus: ISAF-RT (Hoek-Brown) yields E_rm = 23.4 GPa for Zone C (GSI = 70), while the Q-system correlation gives E_m = 17.7 GPa (Q_c = 5.56) — a factor of ~1.3. This difference propagates into the GRC stiffness: a softer rock mass produces a lower GRC slope, higher wall displacement, and a more onerous SCC convergence requirement. The ISAF-RT value is more consistent with laboratory measurements on intact Tithonian limestone (E_i = 65 GPa) at GSI = 70.

8.3 Integrated Application Strategy

Despite the quantitative discrepancy in Zone C, the Q-system retains practical value as a real-time face-mapping tool during construction, complementary to the pre-design ISAF-RT framework. The following three-stage integration strategy is proposed for future tunnel projects in the Gorges du Verdon and analogous Subalpine fold-and-thrust belt settings:

Stage 1 — Pre-Design (3–5 years before construction): Full ISAF-RT Phase I–III stress characterisation via 3 pilot boreholes (600–900 m each) with ELOTs at 50-m depth intervals and

ATV logging; 3D structural mapping using LiDAR and photogrammetry; laboratory testing (UCS, Brazilian, triaxial); probabilistic stress model with P10-P50-P90 Monte Carlo bounds (N = 10,000 realisations); critical zone identification (Phase II RSI screening); and pre-design support selection (Phase V CCM). Estimated investigation cost: €1.2–1.8 M.

Stage 2 — During Excavation (Observational Method): Systematic Q-system logging at every 2-m advance cycle; Q-values mapped in 3D GIS with deviations > 20% from pre-design triggering ISAF-RT Phase VI feedback loop; convergence monitoring at 5-m intervals via total stations and fibre-optic sensors; when K_0 back-calculated from convergence exceeds 1.4, escalate to ISAF-RT-grade support design.

Stage 3 — Post-Construction and Long-Term: Annual convergence readings for 10 years (Phase VI long-term stability); stress model update using as-built convergence database; lining reliability assessment against P90 stress scenario after 50 years. Estimated cost savings from adaptive feedback: reduction of heavy support quantities in ~30% of tunnel length, equivalent to €8–12 M for a 4.6-km tunnel of this type.

9. Discussion

9.1 Implications of the Thrust-Regime Stress State

The most significant geomechanical implication of the present analysis is the confirmation that the Castellane fold-and-thrust belt operates under a thrust-faulting stress regime throughout the T-VD1 alignment ($K_0 > 1.35$ at H = 470 m). This is physically consistent with the active shortening documented by Cardinal et al. (2024) — uplift of ~0.10 mm/yr and ongoing thin-skin compression — and with the geologically recent Digne-Castellane thrust system. The stress regime does not transition to strike-slip or normal faulting at the depths analysed, in contrast to many Shield-type environments where K_0 decays toward 1.0 below ~200–300 m.

The consequence is that the vertical stress S_v is always the minimum principal stress, and the critical loading direction is horizontal, perpendicular to the gorge axis. The Kirsch springline stress concentration (σ_θ,max = 51.68 MPa at Zone C) exceeds the rock mass compressive strength (σ_cm = 23.5 MPa) by a factor of 2.2 — a condition that would not be anticipated from overburden depth alone (H = 470 m, S_v = 12.22 MPa < σ_cm), illustrating the critical role of $K_0 > 1$ in controlling tunnel stability at depth.

These findings are consistent with the broader literature on Alpine stress regimes. Sternai et al. (2019) demonstrate ongoing post-glacial isostatic rebound and tectonic shortening in the SW Alps contributing to elevated horizontal stresses. Schwartz et al. (2017) show that crustal thickening in the Western Alps sustains orogenic stresses at mid-crustal depths. The Sheorey (1994) model, calibrated against measurements in compressional tectonic environments, provides physically grounded K_0 estimates (1.35–1.75 at H = 80–470 m) that are broadly compatible with the limited published in situ stress data from the SE French Alps.

9.2 The Role of Glacial Incision History in Geomechanical Design

Cardinal et al. (2024)'s ^{36}Cl cosmogenic dataset reveals a deglaciation flood pulse at 16–15 ka generating incision rates of 0.90 ± 0.53 mm/yr — 5–9 times the long-term average of ~0.10 mm/yr. This transient event carved the final deepening of the Samson Corridor section of the gorge. From a geomechanical perspective, this rapid unloading may have contributed to three enduring effects on the rock mass.

First, stress relaxation parallel to the gorge walls: the rapid release of confinement perpendicular to the canyon walls during incision may have created a secondary stress relief zone within 20–50 m of the gorge walls, most relevant to the portal Zone A. Second, reactivation of E-W joints: rapid tension cracking during deglaciation flood events promoted the development of sub-vertical E-W open joints at the canyon rim, reducing the effective GSI from table values (70 → 55) within 30–50 m of the surface. Third, karst development: the sustained high-discharge post-glacial period promoted dissolution along pre-existing fractures, creating preferential drainage paths that affect J_w values and groundwater management requirements throughout the tunnel alignment.

These glacially-driven heterogeneities are more effectively captured by ISAF-RT Phase VI long-term assessment — which models historical stress path changes and their impact on lining reliability — than by the Q-system, which treats J_w as a static parameter without temporal evolution. The ISAF-RT framework provides a natural vehicle for incorporating paleo-stress reconstructions such as those enabled by the ^{36}Cl dataset of Cardinal et al. (2024).

9.3 Limitations and Uncertainties

The present analysis is based on a hypothetical tunnel scenario (T-VD1); no actual borehole data, ELOT measurements, or field stress determinations exist for the HVG. The key sources of uncertainty are as follows. (i) Stress tensor orientation: S_Hmax orientation (N130-150°E assumed) may deviate locally due to topographic stress perturbations near the gorge walls (Martel, 2011). A ±25° sensitivity on S_Hmax orientation would change σ_θ,max at Zone C by ±15–20%. (ii) GSI assignments: the values in Table 3 (45–70) span the typical range for Alpine limestone; actual site values may differ by ±10 units, changing σ_cm by ±30% and ε_s by ±50%. (iii) Pore pressure distribution: the assumed hydrostatic water table creates significant effective stress uncertainty; a 100-m drawdown through tunnel drainage would reduce effective S_hmin by ~1.0 MPa, easing the squeezing risk. (iv) K_0 at shallow depth: the Sheorey model at H < 150 m may over-predict K_0; field evidence from Vaucluse and Dauphiné analogues suggests $K_0 \leq 2.5$ at H = 80–100 m in Alpine carbonates.

These uncertainties reinforce the necessity of the Phase I field investigation campaign prescribed by ISAF-RT. Such a campaign would reduce K_0 uncertainty from ±0.40 (current P10-P90 bounds) to ±0.12 (post-ELOT campaign), transforming the analysis from indicative to design-grade. The three-stage observational strategy outlined in Section 8.3 provides the operational framework for implementing this improvement programme.

10. Conclusions

This paper has applied the ISAF-RT integrated stress analysis framework (Calvi, 2026) to a hypothetical road tunnel through the Gorges du Verdon, grounded in the detailed geomorphological and geological dataset of Cardinal et al. (2024) for the High Verdon Gorges. The principal conclusions are the following.

1. The Castellane fold-and-thrust belt is characterised by a thrust-faulting stress regime throughout the T-VD1 alignment, with K_0 = 1.35–1.75 at H = 470 m. The active tectonic setting — documented by ^{36}Cl incision chronology (uplift ~0.10 mm/yr, ongoing thin-skin compression) — generates horizontal stresses 35–75% above the vertical overburden stress, precluding the use of any method that assumes $K_0 \approx 1$.
2. The deep central section (Zone C, H = 470 m, Tithonian limestone, GSI = 70) is the critical design zone: RSI = 0.37, Kastner plastic zone R_p/R = 1.62, squeezing index ε_s = 10–13%

(high to severe), and required support capacity P_i = 0.62–0.83 MPa. The recommended support is a ductile SFRS ring with yielding slots and a 450-mm reinforced concrete secondary lining, with strict zero-passage rules and a 2:1 Factor of Safety.

3. The portal section (Zone A, H = 100 m) presents a counter-intuitive severe squeezing risk (ε_s = 18.4%) due to the low rock mass strength of the highly fractured Berriasian-Hauterivian limestone (σ_cm = 3.8 MPa), which barely exceeds the far-field mean stress. This risk is correctly flagged by ISAF-RT Phase II RSI screening but would not be anticipated from Q-system classification alone.

4. Barton's Q-system under-predicts support demand by a factor of 2.1–2.2 in Zone C relative to ISAF-RT. The discrepancy is rooted in the Q-system's empirical SRF formulation, calibrated against isotropic-stress case histories, which lacks the physical resolution of the Kirsch-Kastner-Hoek-Brown chain in capturing the full stress tensor orientation and magnitude. Implementing only Q-system support in Zone C would result in lining overstress and potential collapse during the construction phase.

5. The two methods are complementary rather than competing: ISAF-RT provides the rigorous pre-design stress model and critical zone identification; the Q-system provides a fast, operationally practical real-time face-logging system during construction. The three-stage integration strategy proposed in Section 8.3 optimises the respective strengths of both approaches across the project lifecycle.

6. The ^{36}Cl incision chronology of Cardinal et al. (2024) provides critical geomechanical constraints: the 16–15 ka flood pulse (incision rate 0.90 ± 0.53 mm/yr) created transient unloading episodes that may have degraded GSI and J_w near the gorge walls, while the long-term 0.10 mm/yr uplift rate confirms the ongoing tectonic compression sustaining the high K_0 stress state. The ISAF-RT Phase VI long-term assessment provides a natural framework for incorporating this paleo-stress history.

7. In tectonically active fold-and-thrust belts — including the Verdon, Durance, and Var gorges of the SW French Alps, and analogous settings in the Apennines, Pyrenees, and Zagros — explicit stress regime characterisation following the ISAF-RT protocol is indispensable for safe and economical underground design. The empirical K_0 assumptions underlying conventional classification-based design are systematically non-conservative in such environments.

References

Barton, N. (2002). Some new Q-value correlations to assist in site characterisation and tunnel design. International Journal of Rock Mechanics and Mining Sciences, 39(2), 185–216. https://doi.org/10.1016/S1365-1609(02)00011-4.

Barton, N., Lien, R., Lunde, J. (1974). Engineering classification of rock masses for the design of tunnel support. Rock Mechanics, 6(4), 189–236.

Brudy, M., Zoback, M.D., Fuchs, K., Rummel, F., Baumgärtner, J. (1997). Estimation of the complete stress tensor to 8 km depth in the KTB scientific drill holes. Journal of Geophysical Research, 102(B8), 18453–18475.

Byerlee, J. (1978). Friction of rocks. Pure and Applied Geophysics, 116, 615–626.

Calvi, A. (2026). In-Situ Stress State in Rock Masses and Its Application to Road and Railway Tunnel Excavation: Integrating Reservoir Geomechanics with a New Analytical Framework (ISAF-RT). Journal of Rock Mechanics and Tunnelling Technology (JRMTT). SSRN Working Paper 7145618. https://ssrn.com/abstract=7145618. https://doi.org/10.2139/ssrn.7145618.

Cardinal, T., Petit, C., Rolland, Y., Schwartz, S., Valla, P.G., Scalabrino, B., Audin, L., Bertauts, M., Zerathe, S., Thiéblemont, D., Braucher, R., ASTER Team (2024). The interplay of geology, climate and tectonics on river incision: the example of the High Verdon Gorges, Southwestern French Alps. Comptes Rendus Géoscience, 356 (Special Issue S2), 265–287. https://doi.org/10.5802/crgeos.216.

Carranza-Torres, C., Fairhurst, C. (1999). The elasto-plastic response of underground excavations in rock masses that satisfy the Hoek-Brown failure criterion. International Journal of Rock Mechanics and Mining Sciences, 36(6), 777–809.

CIRIA (1999). The Observational Method in Ground Engineering: Principles and Applications. Report C185. CIRIA, London.

Grimstad, E., Barton, N. (1993). Updating of the Q-system for NMT. Proceedings International Symposium on Sprayed Concrete, Oslo. Norwegian Concrete Association, 46–66.

Hoek, E., Carranza-Torres, C., Corkum, B. (2002). Hoek-Brown failure criterion — 2002 edition. Proceedings NARMS-TAC Conference, Toronto, 267–273.

Hoek, E., Marinos, P.G. (2000). Predicting tunnel squeezing. Tunnels and Tunnelling International, 32(11), 45–51; 32(12), 34–36.

Kaiser, P.K., McCreath, D.R., Tannant, D.D. (1996). Canadian Rockburst Support Handbook. Geomechanics Research Centre, Sudbury, Ontario.

Kastner, H. (1962). Statik des Tunnel- und Stollenbaues. Springer, Berlin.

Kirsch, C. (1898). Die Theorie der Elastizität und die Bedürfnisse der Festigkeitslehre. Zeitschrift des Vereines Deutscher Ingenieure, 42, 797–807.

Kovári, K. (1998). Tunnelling in squeezing rock. Tunnel, 5, 12–31.

Marinos, P., Hoek, E. (2000). GSI: a geologically friendly tool for rock mass strength estimation. Proceedings GeoEng2000, Melbourne, 1422–1446.

Martel, S.J. (2011). Mechanics of curved surfaces, with application to surface-parallel cracks. Geophysical Research Letters, 38, L20303.

Panet, M., Guenot, A. (1982). Analysis of convergence behind the face of a tunnel. Proceedings 3rd International Symposium on Tunnelling, IMM, London, 197–204.

Peck, R.B. (1969). Advantages and limitations of the observational method in applied soil mechanics. Géotechnique, 19(2), 171–187.

Sanchez, G., Rolland, Y., Schreiber, D., Giannerini, G., Corsini, M., Lardeaux, J.M. (2010). The active fault system of SW Alps. Journal of Geodynamics, 49(5), 296–302.

Schwartz, S., Gautheron, C., Audin, L., Dumont, T., Nomade, J., Barbarand, J. et al. (2017). Foreland exhumation controlled by crustal thickening in the Western Alps. Geology, 45(2), 139–142.

Sébrier, M., Ghafiri, A., Bles, J.-L. (1997). Paleoseismicity in France: fault trench studies in an intraplate setting. Journal of Geodynamics, 24(1–4), 207–217.

Sheorey, P.R. (1994). A theory for in situ stresses in isotropic and transversely isotropic rock. International Journal of Rock Mechanics and Mining Sciences, 31(1), 23–34.

Sternai, P., Sue, C., Husson, L., Serpelloni, E., Becker, T.W., Willett, S.D. et al. (2019). Present-day uplift of the European Alps: evaluating mechanisms and models. Earth-Science Reviews, 190, 589–604.

Vlachopoulos, N., Diederichs, M.S. (2009). Improved longitudinal displacement profiles for convergence-confinement analysis of deep tunnels. Rock Mechanics and Rock Engineering, 42(2), 131–146.

Zoback, M.D. (2010). Reservoir Geomechanics. Cambridge University Press, Cambridge, UK. ISBN 978-0-521-14619-7.

Zoback, M.D., Barton, C.A., Brudy, M., Castillo, D.A., Finkbeiner, T., Grollimund, B.R. et al. (2003). Determination of stress orientation and magnitude in deep wells. International Journal of Rock Mechanics and Mining Sciences, 40, 1049–1076.